Journal of
Materials Chemistry C

Materials for optical, magnetic and electronic devices

Accepted Manuscript

This article can be cited before page numbers have been issued, to do this please use: J. Chen, J. Li, G. Nedelcu, P. Hansch, L. Di Mario, L. Protesescu and M. A. Loi, *J. Mater. Chem. C*, 2024, DOI: 10.1039/D4TC02404D.

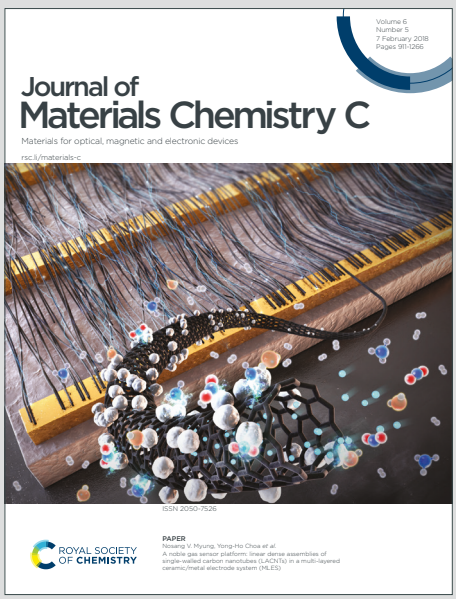

ROYAL SOCIETY OF CHEMISTRY

rsc.li/materials-c

View Article Online
DOI: 10.1039/D4TC02404D

Blade-coated perovskite nanoplatelets polymer composite for sky-blue light-emitting diodes

Jiale Chen[1], Jiaxiong Li[1], Georgian Nedelcu[2], Paul Hansch[1], Lorenzo Di Mario[1], Loredana Protesescu[2], Maria A. Loi*[1]

[1] Photophysics & OptoElectronics, Zernike Institute for Advanced Materials, University of Groningen, Nijenborgh 3, 9747AG, Groningen, The Netherlands
[2] Materials Chemistry, Zernike Institute for Advanced Materials, University of Groningen, Nijenborgh 3, 9747AG, Groningen, The Netherlands
*Corresponding author: M.A.Loi@rug.nl

Abstract

Colloidal perovskite nanoplatelets (NPLs) have shown promises for tackling the blue light-emitting diode challenges based on their tunable band gap and high photoluminescence efficiencies. However, high quality and large area dense NPLs films have proven very hard to prepare because of their chemical and physical fragility during the liquid phase deposition Herein, we report a perovskite-polymer composite film deposition strategy with fine morphology engineering obtained with the blade coating method. The effects on the film quality of polymer type, solution concentration, compounding ratio and film thickness are systematically investigated. We found that a relatively high-concentration suspension with an optimized NPLs to polymer ratio of 1:2 is crucial for the suppression of phase separation and arriving at a uniform film. Finally, sky-blue NPLs-based perovskite light-emitting diodes were fabricated by blade coating showing EQE of 0.12% on a device area of 16 mm^2.

Keywords: Colloidal perovskite nanoplatelets, light-emitting diodes, blade coating, nanocomposite film

View Article Online
DOI: 10.1039/D4TC02404D

1.Introduction

Colloidal lead halide perovskite nanocrystals (PNCs) can be easily synthesized in liquid phase reactions (hot injection) and due to their prominent optoelectronic properties, such as high photoluminescence quantum yield (PLQY), tunable band gap and narrow emission spectra, they are promising materials for the fabrication of light-emitting diodes [1-5]. Specifically, by taking advantage of the precise crystal size control obtained by tuning the parameters of the hot-injection reaction, PNCs and nanoplatelets (NPLs) displaying spectrally stable blue-light emission can be obtained.[5-11] In particular, bromide-based two-dimensional perovskite NPLs have been reported to display a PLQY above 80%, with adjustable emitting wavelength from 425 nm to 520 nm through altering the layer numbers [12-14], showing potential of achieving the same level of performance in phase-pure quasi-2D perovskite thin films[15, 16].

So far, many investigations have been devoted into changing the organic ligands at the PNCs surface to enhance the efficiency of NPLs-based perovskite light-emitting diodes (PeLEDs), since the consensus is that the low electrical conductivity of the organic ligand at the surface is the main limiting factor in device performance[17, 18]. However, few reports have focused on the quality of NPLs thin films, which also determines the device efficiency [19-23]. It is straightforward that to fabricate high-performance blue PeLED, high quality and reproducible thin films are the prerequisites. The film coverage and morphology can be directly associated with the structural integrity of the built-up device and the charge injection and recombination schemes. Previous reports on spin coating deposition methods suggested that NPLs are susceptible to self-aggregation during the film formation process[2, 24-27]. Poor substrate coverage and large NCs agglomerates can often be observed after coating, which could result in high leakage current, low EQE and color stability. This drawback is often regarded as the bottleneck for successful large-area LED manufacturing.

Though most of the top-efficiency PeLEDs were achieved via spin coating, large-area deposition by blade-coating has recently attracted great attention and is deemed more suitable than spin-coating for industrial-scale production, not only because the latter is much more prone to material wasting but also since uneven materials distribution could easily happen during the fast film formation of the composite [28-31]. One notable example of blade coating in the fabrication of large-area sky-blue PeLEDs was demonstrated with an active area of 28 cm^2 [32]. A similar approach has also been used for colloidal PNCs by using an bar-coating process, with which highly efficient green PeLEDs (22.5% EQE) with an area of 102 mm^2 [30] were achieved. Yet to date, it is still a great challenge to blade-coat a conductive thin film (<50 nm) composed by a polymer matrix and perovskite nanoparticles with a homogenous morphology. It should be highlighted that much know-how gained from spin-coating may not be directly transferred to the blade-coating fabrication. One of the most important features is that the latter is in thermodynamic equilibrium with the solvent removal obtained only by tuning the temperature of the substrate. It is also important to note that blade-coated films containing quantum confined perovskite NPLs for blue LEDs are still to be demonstrated.

Our strategy to reach uniform and pinhole-free NPL perovskite thin films, is to blend the NPL with a hole-transport polymer of wide band gap. Using a polymeric matrix can help to stabilize the perovskite nanostructures and enhance the charge transport of the active layer where NPLs still have the original ligands.[19, 22, 33]. In fact, colloidal NPLs are easy to aggregate due to loss of ligands and confinement during the film's formation, which may results in strong non-radiative recombination

View Article Online
DOI: 10.1039/D4TC02404D

and inadequate film morphology. [21, 33, 34] In 2016, Gao and colleagues used poly(ethylene oxide) to obtain small microcrystalline perovskite domains and pinhole-free surface and realized high-efficiency green PeLEDs[35]. Zhong and co-workers have shown that using polyvinylidene fluoride improves both PL properties and air stability of the nanocrystal/polymer composite film[36]. Jiang and co-workers used this strategy to prepare a $FAPbI_3$ quantum dot composite film with poly(methyl methacrylate) showing no microscopic aggregation with minor red-shift in PL from 529nm to 534nm [33]. However, there is very little or no success reported on the use of NPLs-polymer composites for PeLEDs.

In this work, we demonstrate a convenient strategy for preparing uniform and non-aggregated blue-emitting $CsPbBr_3$ NPLs/polymer composite thin films via blade-coating at room temperatures. Two very common hole transport tpolymerss, namely, poly(9-vinylcarbazole) (PVK) and poly(4-butyl-N,N-diphenylamine) (P-TPD), were each used as a matrix to form corresponding composite films with NPLs. Important factors, including the selection of the polymer, the concentration of solution, the ratio of NPLs to polymer, and the composite film thickness, are systematically investigated, aiming for a homogeneous morphology by blade-coating[37]. Our study revealed that using a compatible polymer in a highly concentrated suspension is indispensable for suppressing phase separation and forming conformal and compact films. The optimal ratio and concentration of NPLs and P-TPD yielded promising electroluminescence properties leading to PeNPLsLED devices with EQE of 0.12% at 16 mm^2 area. The electrical properties and photophysics of these high-quality films are discussed in relationship with the device performances.

2. Results and discussion

In this work, $CsPbBr_3$ NPLs were synthesized following a procedure reported elsewhere (consult the SI for the detailed procedure) [38, 39]. Figure 1a shows the optical properties of our NPLs measured in suspension showing 72% photoluminescence quantum yield (PLQY). Figure 1b schematically depicts the steps involved in the ink preparation and deposition process to obtain the thin films. The ink is made by mixing freshly synthesized NPLs (see experimental section in SI) bearing oleic acid and oleylamine ligands with the polymer at specific ratios) and concentration under nitrogen atmosphere. The blade-coating setting and the concentration of NPLs solution can significantly affect the morphology of the nanocomposite films, which we will discuss below.

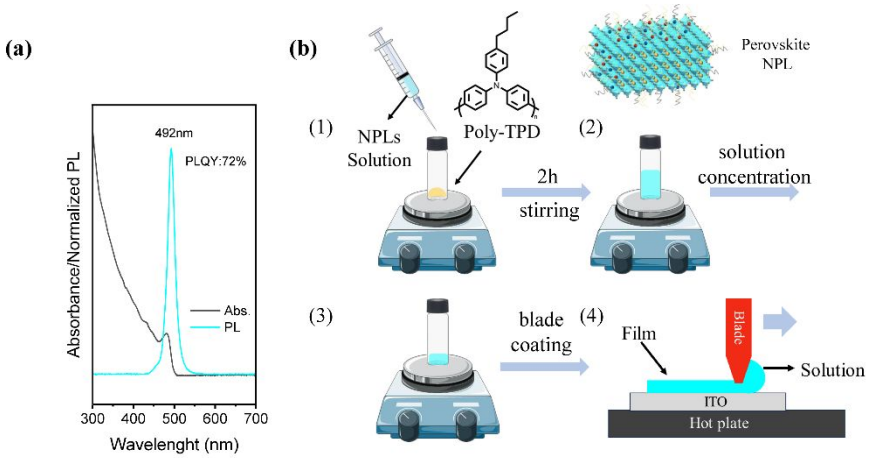

Figure 1. (a) Absorption and PL spectra of $CsPbBr_3$ NPLs. (b) Schematic representation for polymer/ NPLs composite solution preparation (ink) and the doctor-blading process for

View Article Online
DOI: 10.1039/D4TC02404D

deposition.

Many reports have found that closed NPLs films were very hard to prepare starting from low-concentration solutions [18, 40] such as 5mg/mL. However, when increasing the concentration of NPLs suspension from 5mg/mL to 20mg/mL, severe aggregation and followed by precipitation of the NPLs is observed. In our experiments, two different concentrations of NPLs suspensions (5mg/mL and 15mg/mL) were prepared to investigate their film formation behavior in blade coating. The optical-microscopy study revealed aggregation behavior in the film prepared by the high-concentrated suspensions (Figure S1). We, therefore, seek to select a proper conductive polymer that can provide a conductive matrix to embed the NPLs and that is soluble in the same solvent.

Common HTL materials, such as PVK and P-TPD were selected as the matrix since both have a high electrical conductivity and good energy level matching with NPLs[41] to form a type one heterostructure. Their solubility in toluene assists a facile blending with NPLs in the solvent of choice. Atomic Force Microscopy (AFM) was used to study the morphology of blade-coated films from NPLs blends with different polymers. The topography of films deposited from a NPLs-PVK inks (10mg/mL for NPLs and 5mg/mL for PVK) (Figure 2a) exhibit serious phase separation with many randomly distributed islands of round shape, which are probably composed of polymer. When the concentration of PVK is increased from 5 mg/mL to 30 mg/mL (Figure 2b), the phase separation is not improved, but the size of the polymer islands increased from 300 nm to 1μm on average. Therefore, regardless of the starting ratio, the combination between PVK and the perovskite NPLs doesn't lead to homogeneous films. In the case of P-TPDP-TPD-based thin films, similar phase-separation is observed for low concentrations of P-TPDP-TPD (5mg/mL), Figure 2c, but the morphology of these samples appeared substantially different than the one of the samples based on PVK, showing more dendritic like polymer structures. However, when the concentration of P-TPD is increased from 5 mg/mL to 30 mg/mL, the film quality notably improves, showing a rather homogeneous and compact morphology, displayed in Figure 2d. This observation is in line with other studies reporting dramatically different morphologies of colloidal PNCs when spin-coated on PVK or P-TPD layers[42]. Such a drastic difference was mainly attributed to the better affinity of P-TPD towards the NCs ligands, contributing to increase the miscibility of the hetero-phases at high polymer concentration. At the same time, the mixing of the NPLs with PVK may be limited by its bulky side groups. These favorable behaviors recommend P-TPD as the preferred candidate for compounding with perovskite NPLs. Therefore, we carried out further optimizations of NPLs/P-TPD systems, and we focused on understanding the critical parameters determining the film morphology, the absolute concentration of polymer and NPLs, and the polymer-to-NPLs ratio.

View Article Online
DOI: 10.1039/D4TC02404D

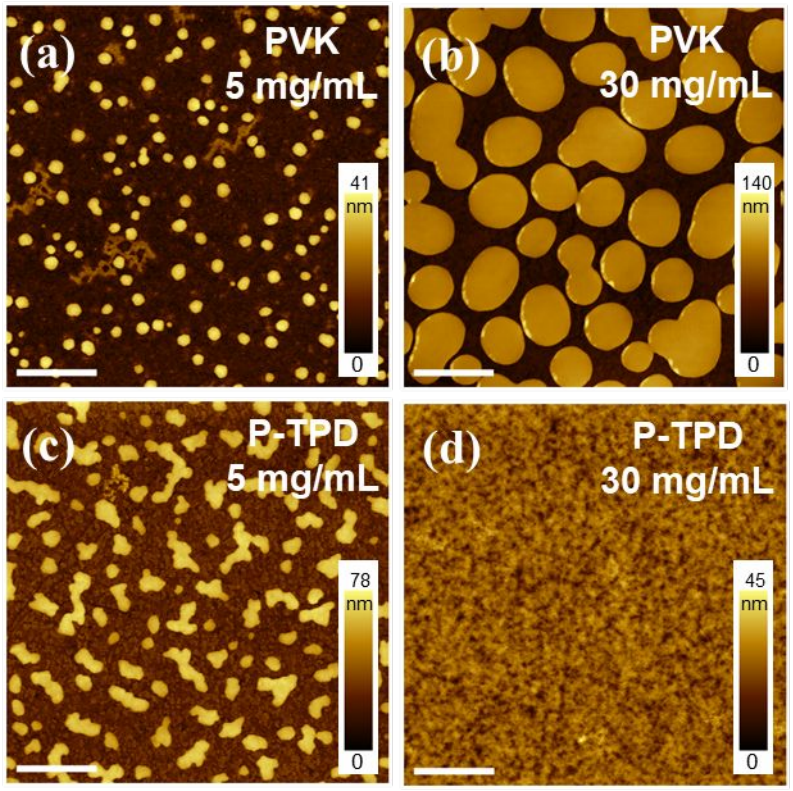

Figure 2. AFM surface topography of the blade-coated films with different ratio of polymers at 10mg/mL NPLs concentration. (a) PVK at 5 mg/mL; (b) PVK at 30mg/mL; (c) P-TPD at 5 mg/mL and (d) P-TPD at 30mg/mL. All the white scale bars represent 2μm.

In the blade-coating process, the concentration of the suspension can have a significant effect on the solvent evaporation rate and rheological behavior, all being important parameters which affect the morphology of the formed film[28, 30, 43]. Suspensions with NPLs concentrations of 2.5mg/mL, 5mg/mL, 10mg/mL, and 15mg/mL with a fixed NPLs to polymer ratio of 1:2 were prepared and used to investigate this phenomenon. All the samples were blade-coated with the same speed and blade height, and the corresponding AFM micrographs are reported in Figure 3. As shown in Figure 3a, an uneven surface showing scattered holes of different sizes was observed for films using low-concentration NPLs (2.5mg/mL). AFM images in Figure S2 indicate that aggregates of NPLs are most probably located inside the holes. We believe this results from a combination of incomplete film coverage and the self-aggregation properties of NPLs at low concentrations. When increasing the solution concentration from 2.5 mg/mL to 5 mg/mL and 10 mg/mL, the number of the holes gradually decreases, and their diameter also decreases as shown in Figures 3b and 3c. Finally, at 15 mg/mL, (Figure 3d) the film shows a smooth and pinhole-free surface. We concluded that blade coating with high-concentration NPLs/polymer blend is essential to obtain continuous films with good morphology.

View Article Online
DOI: 10.1039/D4TC02404D

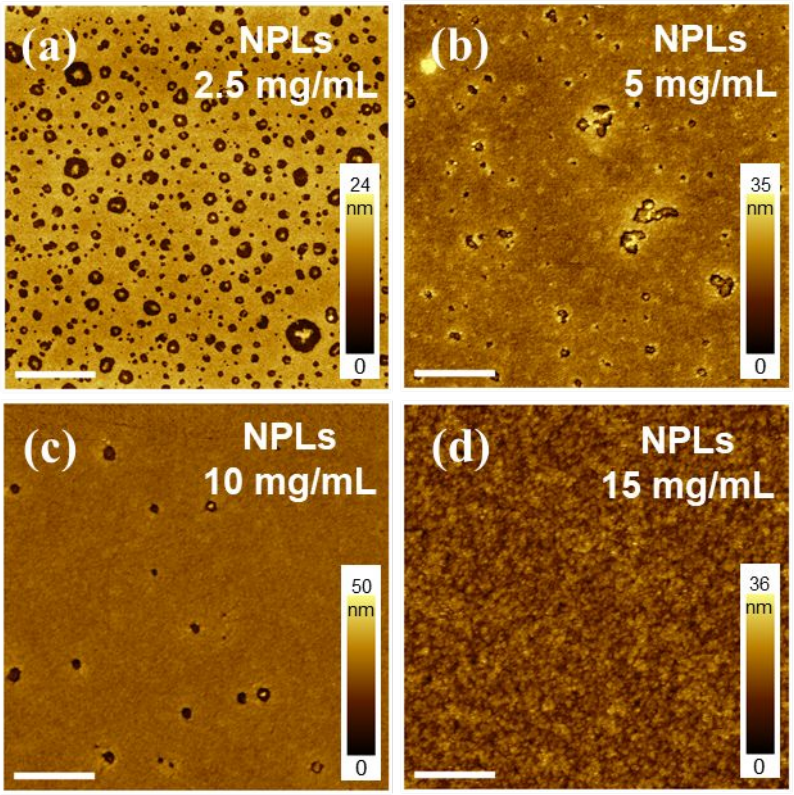

Figure 3. AFM surface morphologies of the blade-coated composite films under fixed NPLs to P-TPD ratio (1:2), with NPLs concentration of (a) 2.5 mg/mL, (b) 5 mg/mL, (c) 10 mg/mL and (d) 15 mg/mL. All white scale bars represent 2μm.

Intuitively, a higher NPL ratio in the binary system is preferred for strong and clean emissions, though clearly the film quality and the NPLs dispersion/connectivity is also expected to strongly determine the device performance. It is thus essential to explore the threshold ratio of NPLs to polymer, above which a well-mixed film cannot be achieved. Based on the concentration optimizations described above (15mg/mL NPLs), we prepared four blends with this concentration and different NPLs to polymer ratios (1:1.6, 1:1.8, 1:2.0, and 1:2.2). The target thickness for films is about 45 nm. As shown in Figure 4a, the composite film blade coated with the 1:1.6 ratio mixture, (polymer concentration of 24 mg/mL) exhibited large holes (diameter ~2μm) on the surface, which is quite different from the low concentration scenario in Figure 3a. This clean-cut and large-scale pinhole formation could be correlated to an insufficient amount of polymer needed to prevent the self-aggregation of high-concentration NPLs. Figure 4b shows that increasing the polymer content to NPLs: P-TPD to 1:1.8, resulted in the disappearance of all pinholes and the composite film showed a well-mixed and homogenous surface. This uniform morphology persisted when we further increased the polymer content to 1:2 an·d 1:2.2 ratio (Figures 4c and 4d). Based on this trend, we consider that a minimum of 1.8 times of NPLs weight of polymer must be included to yield homogeneous blade-coated composite films.

View Article Online
DOI: 10.1039/D4TC02404D

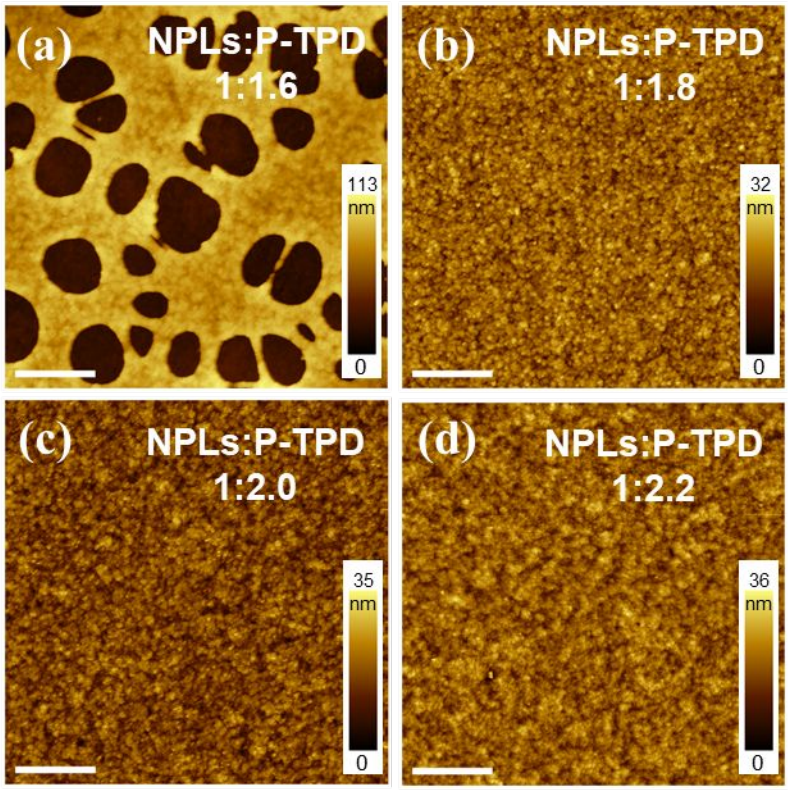

Figure 4. AFM images showing surface morphologies of the blade-coated films using solution with constant NPLs concentration (15mg/mL) and NPLs to P-TPD ratio of (a) 1:1.6, (b)1:1.8, (c)1:2.0 and (d) 1:2.2 with a fixed thickness of 45 nm. All white scale bars represent 2μm.

In general, thinner active layers are favorable for the confinement and radiative recombination of charge carriers in PeLED[44]. In blade coating deposition, the final film thickness can be altered with the solution concentration and by tuning the blading speed. The higher the blading speed, the thicker the films will be obtained, as more ink remains behind the blade. We perform experiments to demonstrate the effect of blading speed on the film thickness and morphology. From the above optimization, four different thicknesses (15, 20, 30 and 45 nm) of the composited film were obtained using the optimized mixed solution (c(NPLs)=15mg/mL, NPLs to polymer ratio=1:2.0), each at the blading speed of 2mm/s, 3mm/s, 5mm/s and 10mm/s. Their corresponding AFM images are reported in Figure 5. In Figure 5a, the composite film 15nm thick showed a large number of holes of about 1 μm diameter on average on the surface. Under such blading conditions, the fast evaporation of solvents may have mimicked the precipitation kinetics in poorly distributed NPLs suspensions. By increasing the thickness of the film to 20 nm and 30 nm, not only the number of pinholes but also their sizes (300 nm and 200 nm on average, respectively) significantly decreased. Apparently, maintaining the optimal morphology while achieving thinner active layer thickness is very challenging, and only when reaching 45nm (Figure 5d) a homogeneous film can be obtained again. It is expected that for each desired thickness the optimization process described above would give rise to a different optimal ratio among the active layer components.

View Article Online
DOI: 10.1039/D4TC02404D

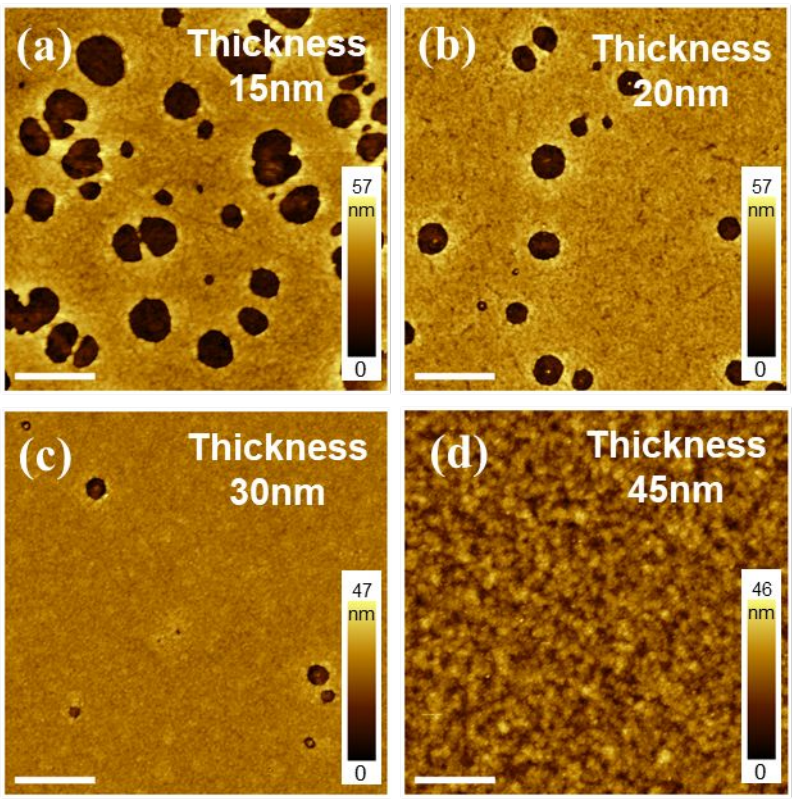

Figure 5. Under a fixed concentration of NPLs (15mg/mL) and a ratio of NPLs to P-TPD (1:2), AFM surface morphologies of the blade-coated films with different thicknesses of (a) 15nm, (b) 20nm, (c) 30nm, (d) 45nm. All white scale bars represent 2μm.

Before attempting the fabrication of light emitting devices, is important to measure the photoluminescence properties of the NPLs-polymer composite film. Four composite films with different P-TPD ratios (1:1.6, 1.8, 2.0 and 2.2) were prepared by the same blade coating condition. The steady state PL (Figure 6a) shows that for all the films the emission spectrum is dominated by a peak at around 495nm, consistent with the PL measurements of the NPLs in solution. However, the spectrum shows a second peak at lower energy, which may derive from energy transfer to a different population of NPLs of slightly different size. Furthermore, the steady state PL (Figure 6a) shows that a peak at about 430nm is present in the spectrum for all the samples and it is increasing intensity as the amount of P-TPD from ratio NPLs: P-TPD increases from 1:1.6 to 1:2.22. Since the concentration of P-TPD increases with the ratio while the concentration of NPLs is fixed, the peak is attributed to the emission from P-TPD. In Figure 6b we report the time resolved PL of the different NPLs: P-TPD concentration. The lifetime of the photoluminescence can be indicative of the quality of the film, interaction between the components and the status of aggregation of the nanoplatelets therein. The decay time of the NPLs PL signal at 495nm (Figure 6b) shows a dependence on their concentration in the film, decreasing faster as the ratio increases. Four composite films with different P-TPD ratios (1:1.6, 1.8, 2.0 and 2.2) were prepared by the same blade coating condition. The PL lifetime of such emission, calculated fitting the experimental data with exponential decay, is 1.39ns, 1.32ns, 1.29ns and 0.79ns for ratios of 1:1.6, 1:1.8, 1:2.0 and 1:2.2, respectively. The decrease of the PL lifetime with the ratio together with a substantial unvaried spectral shape, suggests a competition between NPLs and polymer matrix radiative recombination, with a

View Article Online
DOI: 10.1039/D4TC02404D

mechanism of charge or energy transfer possibly involved. A further evidence of energy transfer upon optical excitation can be the comparison of the PL of the blend in solution (see SI Figure S3a and S3b) and in thin film (Figure S3c). While in solution the signals seem to sum, in thin film the polymer intensity is much smaller when interacting with the NPLs. However, no evidence of rise time is evident in the NPLs signal, which could be explain with the short-range transfer (high relative ratio of NPLs). Overall, the PL characterization highlights the importance of optimal nanocomposite mixing towards light-emitting applications. In particular, the PL measurements seem to suggest an upper limit of 1:2.0 for the NPLs: P-TPD ratio, to reduce the contribution of the polymer matrix to the emission.

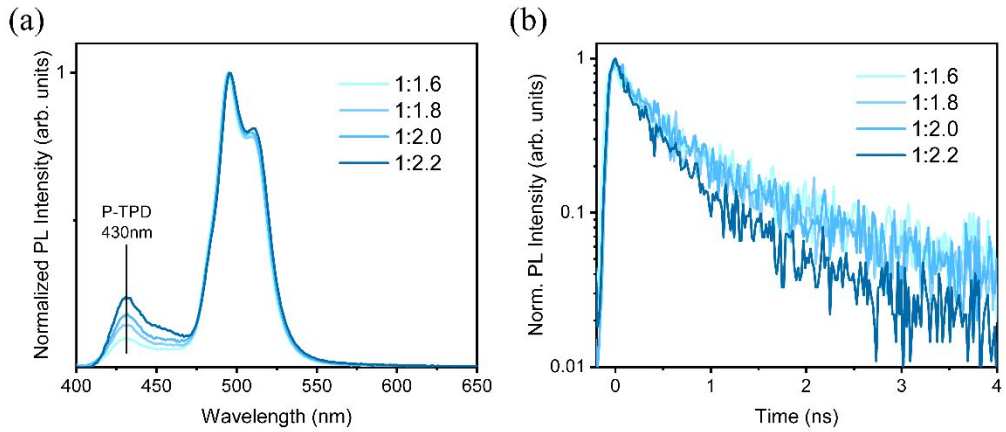

Figure 6. (a) Normalized PL spectra and (b) time-resolved photoluminescence measurement (495nm) of the composite film prepared by constant NPLs concentration (15 mg/mL) and NPLs to P-TPD ratio of 1:1.6, 1:1.8, 1:2.0, and 1:2.2.

From these blade-coated films, PeNPLsLED devices were fabricated utilizing a structure composed of indium tin oxide (ITO)/ PEDOT: PSS (10nm) / the nanocomposite film/ TPBi (35 nm) / LiF (1 nm) / Al (100 nm), as shown in Figure 7a. Figure 7b shows the EL spectra of the optimized device (thickness 45 nm, solution concentration 15 mg/mL and NPLs-polymer ratio of 1:2.0) under the forward bias of 5, 6, 7 and 8 V with the major EL peak located at 492 nm. Interestingly, the EL spectra show less emission from the polymer respect to the PL spectra reported in Figure 6a. We believe this is determined by the recombination occurring directly in the NPLs due to electron and hole injection. The bad conductivity of Poly-TBD for electrons give rise to spurious recombination in the polymer.

LEDs made from suspensions of NPLs (15 mg/mL): Poly-TBD at 1:1.6, and 1:2.0 ratios were adjusted to a thickness of 45 nm. Figure 7c shows the current density-voltage-luminance (J-V-L) curves of a device with area of 16 mm^2. The 1:1.6 device exhibited higher current density at low voltages compared to the other devices made from higher amount of polymer (1:2.0), we believe this difference is determined by some topographic defects in the active layer caused by the penetration of the cathode metal through the device stack. This device showed a maximum EQE of 0.02% and a maximum luminance of 61 cd/m^2 (Figure 7e and 7d), which further increased to maximum EQEs of 0.12% and a maximum luminance of 132 cd/m^2 for the devices with a ratio of 1:2.0. The repeatability of the samples is rather good as shown by the statistics reported in the SI Figure S4. It is important also to notice that the operational stability is limited to few minutes. While the thin films are stable when stored in nitrogen.

View Article Online
DOI: 10.1039/D4TC02404D

It is important to underline that this is one of the first example of a working perovskite NPLs device. The difficulty of finding a proper matrix for blending them, the presence of the ligands on their surface and the fact that the matrix, in this case, is conducting efficiently only holes are all serious limiting factor in achieving higher efficiency. Better results may be expected in the future, if the NPLs could be inserted in between a hole and electron transport layers of large bandgap. However, such a device structure may pose several challenges in term of processability.

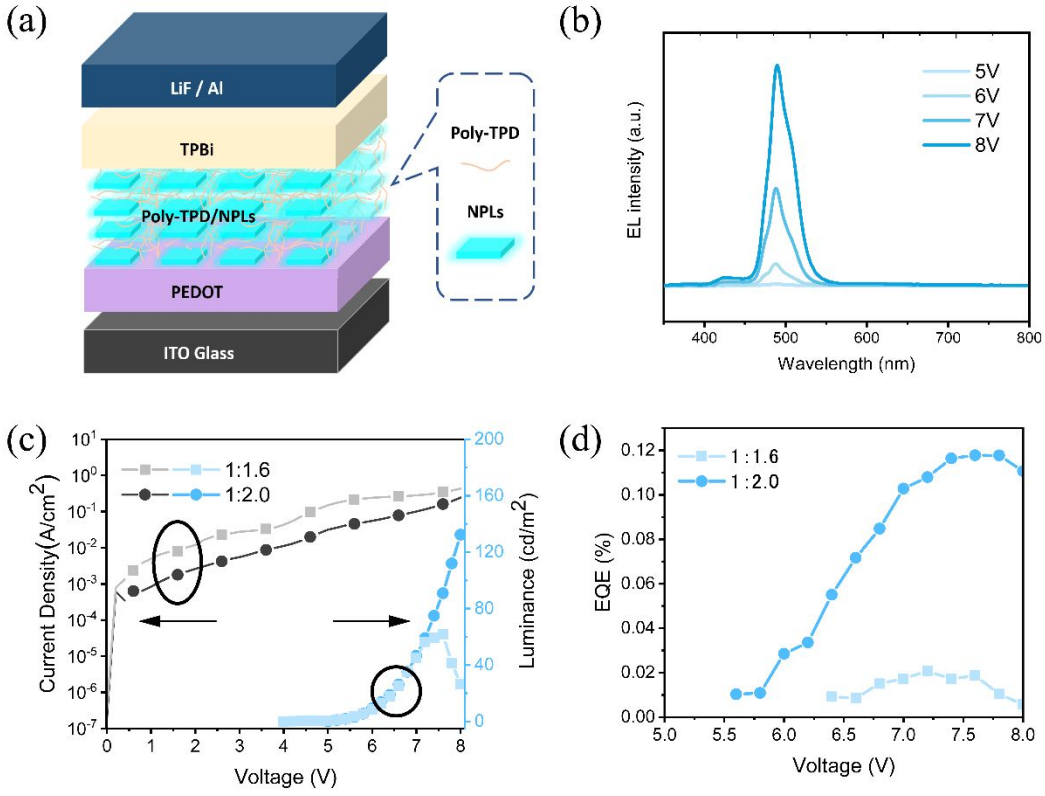

Figure 7. (a) Device structure, (b) EL spectra of the optimized device with the active layer thickness 45nm and prepared from a 15mg/mL NPLs suspension with a polymer mixing ratio of 1:2. (c) Current density-Luminance-voltage curves and (d) EQE--V curves of sky-blue LED with different ratios of NPLs to P-TPD.

5. Conclusion

In conclusion, we developed a nanoplatelet-perovskite-polymer composite film strategy for making uniform blade-coated thin film. The different blade-coating conditions were systematically studied, as well as the selection of polymers, the solution concentration, the ratio of NPLs to polymer and the film thickness, to investigate their corresponding effect on the film formation. Our study revealed that using a high-concentration solution with an optimized NPLs to polymer ratio at 1:2 can be helpful for the suppression of phase separation and allow obtaining films of uniform surface morphology, which is a first pre-condition for the fabrication of LEDs. As a result, the optimized NPLs-based LED shows a sharp emission peak at 492nm with a peak EQE of 0.12% at 16 mm^2 area. Our work highlights the important role of film morphology engineering through designing polymer composites and optimizing blade coating parameters to facilitate the large-scale application of perovskite NPLs in light-emitting solid-state devices.

Acknowledgement

View Article Online
DOI: 10.1039/D4TC02404D

The authors would like to express their gratitude for the technical assistance from Arjen Kamp and Teodor Zaharia. J. Chen appreciates financial funding from Chinese Scholar Council (CSC). This work is funded by the European Union (ERC-AdvancedGrant, DEOM, 101055097). Views and opinions expressed are however those of the author(s) only and do not necessarily reflect those of the European Union or the European Research Council. Neither the European Union nor the granting authority can be held responsible for them.

References

1. C. Otero-Martínez, J. Ye, J. Sung, I. Pastoriza-Santos, J. Pérez-Juste, Z. Xia, A. Rao, R. L. Z. Hoye and L. Polavarapu, *Advanced Materials*, 2021, **n/a**, 2107105.
2. H. Wang, F. Ye, J. Sun, Z. Wang, C. Zhang, J. Qian, X. Zhang, W. C. H. Choy, X. W. Sun, K. Wang and W. Zhao, *ACS Energy Letters*, 2022, DOI: 10.1021/acsenergylett.1c02642, 1137-1145.
3. L. Zhang, C. Sun, T. He, Y. Jiang, J. Wei, Y. Huang and M. Yuan, *Light: Science & Applications*, 2021, **10**, 61.
4. Y. Hassan, J. H. Park, M. L. Crawford, A. Sadhanala, J. Lee, J. C. Sadighian, E. Mosconi, R. Shivanna, E. Radicchi, M. Jeong, C. Yang, H. Choi, S. H. Park, M. H. Song, F. De Angelis, C. Y. Wong, R. H. Friend, B. R. Lee and H. J. Snaith, *Nature*, 2021, **591**, 72-77.
5. Y. Dong, Y.-K. Wang, F. Yuan, A. Johnston, Y. Liu, D. Ma, M.-J. Choi, B. Chen, M. Chekini, S.-W. Baek, L. K. Sagar, J. Fan, Y. Hou, M. Wu, S. Lee, B. Sun, S. Hoogland, R. Quintero-Bermudez, H. Ebe, P. Todorovic, F. Dinic, P. Li, H. T. Kung, M. I. Saidaminov, E. Kumacheva, E. Spiecker, L.-S. Liao, O. Voznyy, Z.-H. Lu and E. H. Sargent, *Nature Nanotechnology*, 2020, **15**, 668-674.
6. H. Liu, M. Worku, A. Mondal, T. B. Shonde, M. Chaaban, A. Ben-Akacha, S. Lee, F. Gonzalez, O. Olasupo, X. Lin, J. S. R. Vellore Winfred, Y. Xin, E. Lochner and B. Ma, *Advanced Energy Materials*, 2022, **n/a**, 2201605.
7. C. Wang, D. Han, J. Wang, Y. Yang, X. Liu, S. Huang, X. Zhang, S. Chang, K. Wu and H. Zhong, *Nature Communications*, 2020, **11**, 6428.
8. Z. Li, Z. Chen, Y. Yang, Q. Xue, H.-L. Yip and Y. Cao, *Nature Communications*, 2019, **10**, 1027.
9. Y. Wu, C. Wei, X. Li, Y. Li, S. Qiu, W. Shen, B. Cai, Z. Sun, D. Yang, Z. Deng and H. Zeng, *ACS Energy Letters*, 2018, **3**, 2030-2037.
10. E.-P. Yao, Z. Yang, L. Meng, P. Sun, S. Dong, Y. Yang and Y. Yang, 2017, **29**, 1606859.
11. A. Q. Liu, C. H. Bi and J. J. Tian, *ADVANCED FUNCTIONAL MATERIALS*, DOI: 10.1002/adfm.202207069.
12. Y. Bekenstein, B. A. Koscher, S. W. Eaton, P. Yang and A. P. Alivisatos, *Journal of the American Chemical Society*, 2015, **137**, 16008-16011.
13. B. J. Bohn, Y. Tong, M. Gramlich, M. L. Lai, M. Döblinger, K. Wang, R. L. Z. Hoye, P. Müller-Buschbaum, S. D. Stranks, A. S. Urban, L. Polavarapu and J. Feldmann, *Nano Letters*, 2018, **18**, 5231-5238.
14. Y. Shynkarenko, M. I. Bodnarchuk, C. Bernasconi, Y. Berezovska, V. Verteletskyi, S. T. Ochsenbein and M. V. Kovalenko, *ACS Energy Letters*, 2019, **4**, 2703-2711.
15. M. J. Rivera Medina, L. Di Mario, S. Kahmann, J. Xi, G. Portale, G. Bongiovanni, A. Mura, J. C. Alonso Huitrón and M. A. Loi, *Nanoscale*, 2023, **15**, 6673-6685.
16. J. Xing, Y. Zhao, M. Askerka, L. N. Quan, X. Gong, W. Zhao, J. Zhao, H. Tan, G. Long, L. Gao, Z. Yang, O. Voznyy, J. Tang, Z.-H. Lu, Q. Xiong and E. H. Sargent, *Nature Communications*, 2018, **9**, 3541.
17. J. Hu, I. W. H. Oswald, S. J. Stuard, M. M. Nahid, N. Zhou, O. F. Williams, Z. Guo, L. Yan, H. Hu, Z. Chen, X. Xiao, Y. Lin, Z. Yang, J. Huang, A. M. Moran, H. Ade, J.

View Article Online
DOI: 10.1039/D4TC02404D

R. Neilson and W. You, *Nature Communications*, 2019, **10**, 1276.
18. W. Shen, Y. Yu, W. Zhang, Y. Chen, J. Zhang, L. Yang, J. Feng, G. Cheng, L. Liu and S. Chen, *ACS Applied Materials & Interfaces*, 2022, **14**, 5682-5691.
19. C. Zhao, P. Liu, W. Cai, W. Xu, M. U. Ali, Z. Xu, H. Y. Fu, H. Meng, J. Li and G. Wei, *Advanced Materials Interfaces*, 2022, **n/a**, 2102212.
20. W. Feng, Y. Zhao, K. Lin, J. Lu, Y. Liang, K. Liu, L. Xie, C. Tian, T. Lyu and Z. Wei, *Advanced Functional Materials*, 2022, **n/a**, 2203371.
21. Y. Xin, H. Zhao and J. Zhang, *ACS Applied Materials & Interfaces*, 2018, **10**, 4971-4980.
22. T. Xuan, J. Huang, H. Liu, S. Lou, L. Cao, W. Gan, R.-S. Liu and J. Wang, *Chemistry of Materials*, 2019, **31**, 1042-1047.
23. H. Wu, S. Wang, F. Cao, J. Zhou, Q. Wu, H. Wang, X. Li, L. Yin and X. Yang, *Chemistry of Materials*, 2019, **31**, 1936-1940.
24. R. L. Z. Hoye, M.-L. Lai, M. Anaya, Y. Tong, K. Gałkowski, T. Doherty, W. Li, T. N. Huq, S. Mackowski, L. Polavarapu, J. Feldmann, J. L. MacManus-Driscoll, R. H. Friend, A. S. Urban and S. D. Stranks, *ACS Energy Letters*, 2019, **4**, 1181-1188.
25. C. Bi, S. Wang, S. V. Kershaw, K. Zheng, T. Pullerits, S. Gaponenko, J. Tian and A. L. Rogach, *Advanced Science*, 2019, **6**, 1900462.
26. Y. Ling, Z. Yuan, Y. Tian, X. Wang, J. C. Wang, Y. Xin, K. Hanson, B. Ma and H. Gao, 2016, **28**, 305-311.
27. D. Liang, Y. Peng, Y. Fu, M. J. Shearer, J. Zhang, J. Zhai, Y. Zhang, R. J. Hamers, T. L. Andrew and S. Jin, *ACS Nano*, 2016, **10**, 6897-6904.
28. Z. Zhang, J. Shang, H. Ge, Y. Zhang, L. Zhou, W. Zhu, D. Chen, J. Zhang, C. Zhang and Y. Hao, *Materials Today Energy*, 2023, **36**, 101343.
29. K. Wang and L. Dou, *Nature Nanotechnology*, 2022, **17**, 562-563.
30. Y.-H. Kim, J. Park, S. Kim, J. S. Kim, H. Xu, S.-H. Jeong, B. Hu and T.-W. Lee, *Nature Nanotechnology*, 2022, DOI: 10.1038/s41565-022-01113-4.
31. M. Remeika and Y. Qi, *Journal of Energy Chemistry*, 2018, **27**, 1101-1110.
32. S. Chu, Y. Zhang, P. Xiao, W. Chen, R. Tang, Y. Shao, T. Chen, X. Zhang, F. Liu and Z. Xiao, *Advanced Materials*, 2022, **34**, 2108939.
33. H. Zhu, M. Cheng, J. Li, S. Yang, X. Tao, Y. Yu and Y. Jiang, *Chemical Engineering Journal*, 2022, **428**, 130974.
34. K. Hoshi, T. Chiba, J. Sato, Y. Hayashi, Y. Takahashi, H. Ebe, S. Ohisa and J. Kido, *ACS Applied Materials & Interfaces*, 2018, **10**, 24607-24612.
35. Y. Ling, Y. Tian, X. Wang, J. C. Wang, J. M. Knox, F. Perez-Orive, Y. Du, L. Tan, K. Hanson, B. Ma and H. Gao, *Advanced Materials*, 2016, **28**, 8983-8989.
36. Q. Zhou, Z. Bai, W.-g. Lu, Y. Wang, B. Zou and H. Zhong, *Advanced Materials*, 2016, **28**, 9163-9168.
37. S. G. R. Bade, X. Shan, P. T. Hoang, J. Li, T. Geske, L. Cai, Q. Pei, C. Wang and Z. Yu, *Advanced Materials*, 2017, **29**, 1607053.
38. M. Vasilopoulou, A. Fakharuddin, F. P. García de Arquer, D. G. Georgiadou, H. Kim, A. R. b. Mohd Yusoff, F. Gao, M. K. Nazeeruddin, H. J. Bolink and E. H. Sargent, *Nature Photonics*, 2021, **15**, 656-669.
39. G. Nedelcu, DOI: 10.3929/ethz-b-000369809, ETH Zurich, 2019.

40. J. A. Sichert, Y. Tong, N. Mutz, M. Vollmer, S. Fischer, K. Z. Milowska, R. García Cortadella, B. Nickel, C. Cardenas-Daw, J. K. Stolarczyk, A. S. Urban and J. Feldmann, *Nano Letters*, 2015, **15**, 6521-6527.
41. S. Peng, S. Wang, D. Zhao, X. Li, C. Liang, J. Xia, T. Zhang, G. Xing and Z. Tang, *Small Methods*, 2019, **3**, 1900196.
42. Z. L. Tseng, L. C. Chen, L. W. Chao, M. J. Tsai, D. A. Luo, N. R. Al Amin, S. W. Liu and K. T. Wong, *ADVANCED MATERIALS*, 2022, **34**.
43. Y. Zhong, R. Munir, J. Li, M.-C. Tang, M. R. Niazi, D.-M. Smilgies, K. Zhao and A. Amassian, *ACS Energy Letters*, 2018, **3**, 1078-1085.
44. Z.-K. Tan, R. S. Moghaddam, M. L. Lai, P. Docampo, R. Higler, F. Deschler, M. Price, A. Sadhanala, L. M. Pazos, D. Credgington, F. Hanusch, T. Bein, H. J. Snaith and R. H. Friend, *Nature Nanotechnology*, 2014, **9**, 687-692.

Data are available upon request from the authors.

View Article Online
DOI: 10.1039/D4TC02404D